

Ruimin Wang,<sup>a,b</sup> Christian W.  
Lehmann<sup>b</sup> and Ulli Englert<sup>a\*</sup><sup>a</sup>Institute of Inorganic Chemistry, RWTH Aachen University, Landoltweg 1, D-52074 Aachen, Germany, and <sup>b</sup>Max-Planck Institut für Kohlenforschung, Kaiser-Wilhelm-Platz 1, D-45470 Muelheim an der Ruhr, GermanyCorrespondence e-mail:  
ullrich.englert@ac.rwth-aachen.de**Weak interactions in chain polymers  $[M(\mu-X)_2L_2]_\infty$  ( $M = \text{Zn, Cd}$ ;  $X = \text{Cl, Br}$ ;  $L = \text{substituted pyridine}$ ) – an electron density study**

Received 20 January 2009

Accepted 20 July 2009

Dedicated to Professor Peter  
Luger

The experimental electron-density distributions in crystals of five chain polymers  $[M(\mu-X)_2(\text{py})_2]$  ( $M = \text{Zn, Cd}$ ;  $X = \text{Cl, Br}$ ;  $\text{py} = 3,5\text{-substituted pyridine}$ ) have been obtained from high-resolution X-ray diffraction data sets ( $\sin \theta/\lambda > 1.1 \text{ \AA}^{-1}$ ) at 100 K. Topological analyses following Bader's 'Atoms in Molecules' approach not only confirmed the existence of (3, -1) critical points for the chemically reasonable and presumably strong covalent and coordinative bonds, but also for four different secondary interactions which are expected to play a role in stabilizing the polymeric structures which are unusual for Zn as the metal center. These weaker contacts comprise intra- and inter-strand  $\text{C-H}\cdots\text{X}-M$  hydrogen bonds on the one hand and  $\text{C-X}\cdots\text{X}-\text{C}$  interhalogen contacts on the other hand. According to the experimental electron-density studies, the non-classical hydrogen bonds are associated with higher electron density in the (3, -1) critical points than the halogen bonds and hence are the dominant interactions both with respect to intra- and inter-chain contacts.

**1. Introduction**

We have systematically studied the reaction products of pyridine derivatives with the chlorides, bromides and iodides of divalent metals, in particular with zinc and its higher homologues (Hu & Englert, 2001*a,b*, 2002, 2005*a,b*, 2006*a,b*; Hu, Li & Englert, 2003; Hu, Huster & Englert, 2003; Englert & Schiffers, 2006*a,b*; Hu *et al.*, 2007). The vast majority of pyridine adducts to zinc halides are mononuclear and adopt distorted tetrahedral geometry. As for bromides and iodides, we are not aware of any exceptions to this rule. In the case of zinc chlorides, a small number of extended solids with octahedral coordination at the metal have been reported:

(i) Pickhardt and Staub described the two-dimensional network structures of  $[\text{Zn}(\mu\text{-Cl})_2(\mu\text{-pyrazine})]_\infty^2$  and  $[\text{Zn}(\mu\text{-Cl})_2(\mu\text{-pyrimidine})]_\infty^2$  (Pickhardt & Staub, 1996).

(ii)  $[\text{Zn}(\mu\text{-Cl})_2(\text{py})_2]_\infty$  ( $\text{py} = 3,5\text{-dichloropyridine}$ , 3,5-dibromopyridine; Hu & Englert, 2002) and  $[\text{Zn}(\mu\text{-Cl})_2(2\text{-chloropyrazine})_2]_\infty$  (Bhosekar *et al.*, 2008) are the only examples of one-dimensional chain polymers.

(iii)  $[\text{ZnCl}_2(\text{bipyridine})]$  has been shown to be dynamic, with four-coordinated metal centers at high and octahedral coordination at low temperature; both structures may be interconverted *via* a single-crystal to single-crystal reaction (Hu & Englert, 2005*a,b*).

The situation is completely different for cadmium derivatives with the same  $[\text{MX}_2(\text{py})_2]$  stoichiometry: They usually are extended solids with octahedral metal coordination. Simple size criteria can be invoked to explain this different behaviour between  $\text{Zn}^{\text{II}}$  and  $\text{Cd}^{\text{II}}$  compounds in general; however, the

**Table 1**  
Crystal data and data collection parameters.

	(1)	(2)	(3)	(4)	(5)
Chemical formula	C <sub>10</sub> H <sub>6</sub> Cl <sub>6</sub> N <sub>2</sub> Zn	C <sub>10</sub> H <sub>6</sub> Br <sub>4</sub> Cl <sub>2</sub> N <sub>2</sub> Zn	C <sub>14</sub> H <sub>18</sub> Br <sub>2</sub> CdN <sub>2</sub>	C <sub>10</sub> H <sub>6</sub> Br <sub>2</sub> CdCl <sub>4</sub> N <sub>2</sub>	C <sub>10</sub> H <sub>6</sub> Br <sub>6</sub> CdN <sub>2</sub>
<i>M<sub>r</sub></i>	432.24	610.08	486.52	568.19	746.03
Crystal system, space group	Tetragonal, <i>P</i> 4 <i>b</i> 2	Tetragonal, <i>P</i> 4 <i>b</i> 2	Tetragonal, <i>P</i> 4 <i>b</i> 2	Monoclinic, <i>C</i> 2/ <i>m</i>	Tetragonal, <i>P</i> 4 <i>b</i> 2
Temperature (K)	100	100	100	100	100
<i>a</i> , <i>b</i> , <i>c</i> (Å)	13.7958 (4), 13.7958 (4), 3.6371 (2)	13.8260 (2), 13.8260 (2), 3.70440 (10)	14.4457 (3), 14.4457 (3), 3.93450 (10)	20.0345 (5), 20.4024 (6), 3.8561 (2)	14.3513 (2), 14.3513 (2), 3.9082 (2)
β (°)	–	–	–	98.518 (2)	–
<i>V</i> (Å <sup>3</sup> )	692.23 (5)	708.13 (2)	821.04 (3)	1558.80 (10)	804.93 (3)
<i>Z</i>	2	2	2	4	2
Radiation type	Mo <i>K</i> α	Mo <i>K</i> α	Mo <i>K</i> α	Mo <i>K</i> α	Mo <i>K</i> α
μ (mm <sup>-1</sup> )	2.91	13.38	6.19	7.20	16.23
Crystal form, size (mm)	Rod, 0.60 × 0.15 × 0.15	Rod, 0.24 × 0.09 × 0.09	Rod, 0.28 × 0.07 × 0.07	Rod, 0.23 × 0.07 × 0.05	Rod, 0.18 × 0.06 × 0.06
<b>Data collection</b>					
Diffractometer	CCD area detector	CCD area detector	CCD area detector	CCD area detector	CCD area detector
Data-collection method	ω scans	ω scans	ω scans	ω scans	ω scans
Absorption correction	Numerical	Numerical	Numerical	Multi-scan	Multi-scan
<i>T</i> <sub>min</sub> , <i>T</i> <sub>max</sub>	0.241, 0.678	0.151, 0.397	0.276, 0.671	0.278, 0.702	0.158, 0.443
(sin θ/λ) <sub>max</sub> (Å <sup>-1</sup> )	1.144	1.145	1.145	1.112	1.149
No. of measured, independent and observed reflections	54 172, 4347, 3850	35 317, 4284, 3189	45 933, 5146, 3889	39 526, 8536, 6007	42 311, 5090, 4364
Criterion for observed reflections	<i>I</i> > 2σ( <i>I</i> )	<i>I</i> > 2σ( <i>I</i> )	<i>I</i> > 2σ( <i>I</i> )	<i>I</i> > 2σ( <i>I</i> )	<i>I</i> > 2σ( <i>I</i> )
<i>R</i> <sub>int</sub>	0.053	0.074	0.067	0.058	0.049
θ <sub>max</sub> (°)	54.4	54.5	54.5	52.2	54.8
<b>Refinement</b>					
Refinement on	<i>F</i> <sup>2</sup>	<i>F</i> <sup>2</sup>	<i>F</i> <sup>2</sup>	<i>F</i> <sup>2</sup>	<i>F</i> <sup>2</sup>
<i>R</i> [ <i>F</i> <sup>2</sup> > 2σ( <i>F</i> <sup>2</sup> )], <i>wR</i> ( <i>F</i> <sup>2</sup> ), <i>S</i>	0.023, 0.049, 1.09	0.028, 0.050, 1.02	0.026, 0.045, 1.05	0.031, 0.048, 0.96	0.025, 0.051, 1.03
No. reflections	4347	4284	5146	8536	5090
No. of parameters	46	46	47	96	46
H-atom treatment	Constrained†	Constrained†	Constrained†	Constrained†	Constrained†
(Δ/σ) <sub>max</sub>	0.003	0.001	0.001	< 0.0001	0.002
Δρ <sub>max</sub> , Δρ <sub>min</sub> (e Å <sup>-3</sup> )	0.45, -0.38	1.99, -1.23	1.24, -2.62	1.35, -1.61	3.10, -0.86

† Constrained to parent site.

role of 3,5-dihalopyridine in stabilizing the chain polymer structures with Zn<sup>II</sup> cations calls for an explanation. We note that the reaction product of ZnCl<sub>2</sub> with the related *N* donor 2,6-dichloropyrazine adopts the usual mononuclear tetrahedral coordination at zinc (Hu & Englert, 2001*b*). Based on the results of standard diffraction experiments, *i.e.* on entirely geometric criteria, we have discussed weak interatomic interactions potentially involved in the stabilization of the chain polymers. In this work we report our results based on a topological analysis of the electron density obtained from high-resolution X-ray diffraction experiments on five [M(μ-X)<sub>2</sub>(py)<sub>2</sub>]<sub>∞</sub> derivatives of zinc and cadmium; Fig. 1 provides a synopsis of the compounds under study.

We are well aware that even high-quality datasets must meet an obvious challenge with respect to the elemental composition of the compounds under study: They all contain transition elements and heavier halides and hence show an unfavourable ratio between valence and core electrons. The suitability factors *s* (Coppens, 1977) vary from 0.36 for (1) to 0.07 for (5) (see §3) and hence cover the range addressed by Macchi and Sironi as ‘presently affordable’ and beyond the ‘current limit’ (Macchi & Sironi, 2003). An additional

complication arises from the fact that four of the above-mentioned compounds crystallize in a non-centrosymmetric space group in which the phase of the structure factor constitutes a continuous variable.

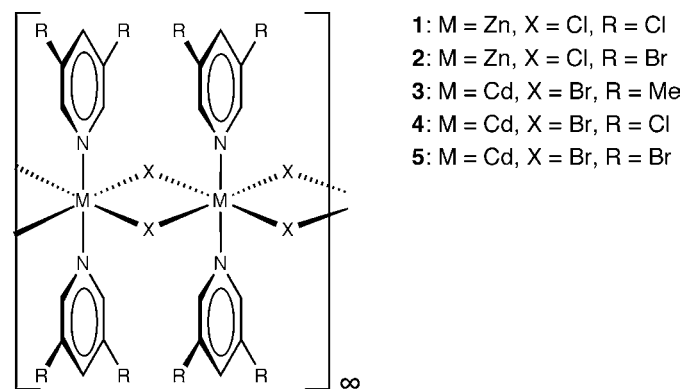


**Figure 1**  
Compounds for which a topological analysis of the electron density has been carried out.

**Table 2**  
Refinement results for the IAM and multipole model.

	(1)	(2)	(3)	(4)	(5)
<b>IAM model</b>					
Function minimized	$F^2$	$F^2$	$F^2$	$F^2$	$F^2$
$R1$ (obs)	0.023	0.028	0.026	0.031	0.025
$R1$ (all)	0.027	0.045	0.041	0.052	0.035
$wR2$ †	0.049	0.050	0.045	0.048	0.048
$a, b$ in weighting scheme	0.021, 0.0	0.015, 0.0	0.01, 0.0	0.01, 0.0	0.017, 0.05
$S$	1.09	1.02	1.05	0.96	1.03
$\Delta\rho_{\max}, \Delta\rho_{\min}$ ( $e \text{ \AA}^{-3}$ )	0.45, -0.38	1.99, -1.23	1.24, -2.62	1.35, -1.61	3.10, -0.86
No. of reflections	4347	4284	5146	8536	5090
No. of parameters	46	46	47	96	46
Packing coefficient (% see text)	76.3	79.0	69.9	71.9	74.1
Flack parameter (Flack, 1983)	0.014 (6)	-0.002 (6)	0.010 (9)	-	0.030 (5)
<b>Multipole model</b>					
Function minimized	$F$	$F$	$F$	$F$	$F$
$R1$ (obs)	0.020	0.024	0.024	0.024	0.021
$R1$ (all)	0.024	0.049	0.046	0.058	0.037
$wR$ ‡	0.018	0.017	0.019	0.016	0.019
$S$	1.747	1.205	1.282	0.962	1.118
$\Delta\rho_{\max}, \Delta\rho_{\min}$ ( $e \text{ \AA}^{-3}$ )	0.109, -0.194	0.406, -0.287	0.372, -0.135	0.511, -0.510	0.456, -0.281
<b>Contraction parameters</b>					
$\kappa$	Refined for all atom types	Fixed to values in (1) for N, Cl <sup>-</sup> and H	Fixed to 0.95 for Cd <sup>2+</sup> , 1.0 for Br <sup>-</sup> , N, C, 1.2 for H	Refined for all atom types	Fixed to values in (1) for N and to 1.2 for H
$\kappa'$ (non-H atoms)	Refined	Fixed to 1.0	Fixed to 1.0	Fixed to 1.0	Fixed to 1.0
$\kappa'$ (H atoms)	Fixed to 1.2	Fixed to 1.2	Fixed to 1.2	Fixed to 1.2	Fixed to 1.2

†  $w^{-1} = \sigma^2(F_o^2) + a \cdot P^2 + b \cdot P$ ;  $P = (F_o^2 + 2F_c^2)/3$ . ‡  $w^{-1} = \sigma^2(F_o^2)$ .

## 2. Experimental

The syntheses of (1) and (2) (Hu & Englert, 2001*a*) and (3)–(5) (Hu & Englert, 2002) have been published earlier, but for the purpose of the present work a different crystallization technique was applied, namely reactant diffusion. Crystals of (1) and (2) were obtained by layering a solution of 1.6 mmol of ZnCl<sub>2</sub> in 20 ml EtOH with a solution of 3.2 mmol of the corresponding pyridine in 20 ml EtOH. Crystals of (3), (4) and (5) were obtained by layering a solution of 0.5 mmol of CdBr<sub>2</sub> in 5 ml dimethylsulfoxide with 1 ml of pure dimethylsulfoxide and, on top of that solvent layer, with 1 mmol of the corresponding pyridine in 5 ml H<sub>2</sub>O. From both categories of diffusion experiments crystals were harvested after several days. Solids (1)–(5) do not melt but rather decompose at 551 [for (1)], 583 [for (2)], 479 [for (3)], 513 [for (4)] and 529 K [for (5)]. The apparent melting of (1) and (2) is in reality associated with the loss of one of the pyridine ligands per metal center (Kalf & Englert, unpublished results).

Intensity data were collected at 100 K with Mo  $K\alpha$  radiation ( $\lambda = 0.71073 \text{ \AA}$ ) on a Bruker D8 goniometer equipped with an APEX CCD detector. The radiation source was either a conventional sealed tube generator [(1)–(4)] or an INCOATEC I- $\mu$ S microsource (5). An Oxford Cryosystems 700 controller was used to ensure constant temperature during data collection. Frames were collected in  $\omega$ -scan mode with three settings for the detector angle  $\theta$  in order to cover low-

order, high-order and intermediate reflections with sufficient overlap between these categories. For each detector setting several runs with different crystal rotation  $\varphi$  were registered. Exposure times varied between 5 and 20 s per frame, depending on crystal size, sample composition and X-ray source. The frames were integrated with the help of the program *SAINT* (Bruker, 2003). Crystals of (1)–(3) and (5) are tetragonal rods elongated along [001] and could reliably be face-indexed; analytical absorption corrections (de Meulenaer & Tompa, 1965) were performed for (1)–(3). In the case of the crystal used for data collection on (5) and also in the case of the less regular crystals (4) multi-scan absorption corrections (Blessing, 1995) proved to be better with respect to merging ( $R_{\text{int}}$ ) and refinement residuals ( $R1, wR2$ ). Both absorption correction methods were used in their *PLATON* (Spek, 2003) implementation. Several attempts were made to avoid rather than to correct absorption: Cutting of rod-shaped crystals after a first data collection resulted in inferior data quality for the second diffraction experiment. Full datasets collected on more isotropic crystals of (5), the compound with the highest linear absorption coefficient, did not reach the resolution and quality criteria associated with the data on the small anisotropic crystal reported below. Crystal data and information concerning data collection and resolution are compiled in Table 1. For the multipole refinements data were merged with *SHELXL97* (Sheldrick, 2008); no outliers were suppressed. Information concerning resolution-dependent averaging of

equivalent reflections and redundancy was obtained with the help of *SORTAV* (Blessing, 1995) and has been compiled in the supporting information.<sup>1</sup>

### 3. Refinement

Refinement on  $F^2$  at the Independent Atom Model (IAM) level was conducted with *SHELXL97* (Sheldrick, 2008). Information on the weighting scheme for each compound is listed in Table 2. Anisotropic displacement parameters were assigned to non-H atoms and H atoms were included in idealized geometry. The packing coefficient is defined as the ratio of occupied to total unit-cell volume (Kitaigorodsky, 1973; Gavezzotti, 1983). This quantity is a simple overall indicator for space-filling efficiency and has been included in Table 2; the values obtained with *PLATON* (Spek, 2003) refer to the following van der Waals radii: C 1.70, H 1.20, N 1.55, Br 1.85, Cl 1.75, Cd 2.49 and Zn 2.25 Å (Bondi, 1964; Spek, 2003). Multipole refinements based on the Hansen–Coppens formalism for aspherical atomic density expansion (Hansen & Coppens, 1978) were carried out with the program *XD2006* (Volkov *et al.*, 2006). Within this program, the SCM databank was used; it contains relativistic wavefunctions for neutral atoms lighter than Kr according to Su & Coppens (1998) and relativistic wavefunctions for neutral atoms from Rb to Xe, as well as for ions as derived by Macchi & Coppens (2001). Statistical weights  $w^{-1} = \sigma^2(F_o^2)$  have been used. With respect to the initial valence electron assignment, metal centers were treated as dicationic  $(n-1)d^{10}ns^0$  systems, the metal-bridging halides as  $ns^2np^6$  monoanions, and the pyridine-bonded halides as neutral atoms with electron configuration  $ns^2np^5$ . Multipole coefficients up to hexadecapoles were refined for non-H atoms. For H atoms, positional coordinates were modified with respect to the IAM model and constrained to match C–H bond distances of 1.083 Å, and monopoles and bond-oriented dipoles were considered in the multipolar refinements.

The refinement of contraction parameters merits a short discussion. As a general strategy, free parameter refinement was attempted; alternatively, parameters obtained from the best and most suitable data sets were transferred to the refinement of chemically related compounds. In detail: For (1), which features the most favourable suitability factor, contraction parameters  $\kappa$  for all atom types and  $\kappa'$  for non-H atoms were freely refined. For the other compounds,  $\kappa'$  of non-H atoms was fixed to 1 and  $\kappa'$  of H atoms to 1.2. In the refinement of (2),  $\kappa$  for N, Cl<sup>−</sup> and H were fixed to the values obtained for (1). During refinement of (3),  $\kappa$  of 0.95 for Cd<sup>2+</sup>, 1.0 for Br<sup>−</sup>, N and C and 1.2 for H were used. In the case of (4),  $\kappa$  for all atom types were freely refined. For (5),  $\kappa$  for N was fixed to the value obtained for (1) and  $\kappa$  for H was fixed to 1.2. Information concerning contraction parameters has also been compiled in Table 2.

<sup>1</sup> Supplementary data for this paper are available from the IUCr electronic archives (Reference: SO5025). Services for accessing these data are described at the back of the journal.

Table 2 also provides a comparison of convergence results at the IAM and multipole refinement level. We note that  $wR2$ , *i.e.* the residual based on  $F^2$ , was the function minimized in the former whereas the latter aimed at minimization of  $wR$ , *i.e.* of structure factors rather than intensities. Residual electron-density information both at the IAM and at the multipole level were obtained by difference-Fourier syntheses based on the complete dataset.

### 4. Results and discussion

Compounds (1)–(5) are one-dimensional coordination polymers. In all compounds chains of halide-bridged  $M^{II}$  octahedra

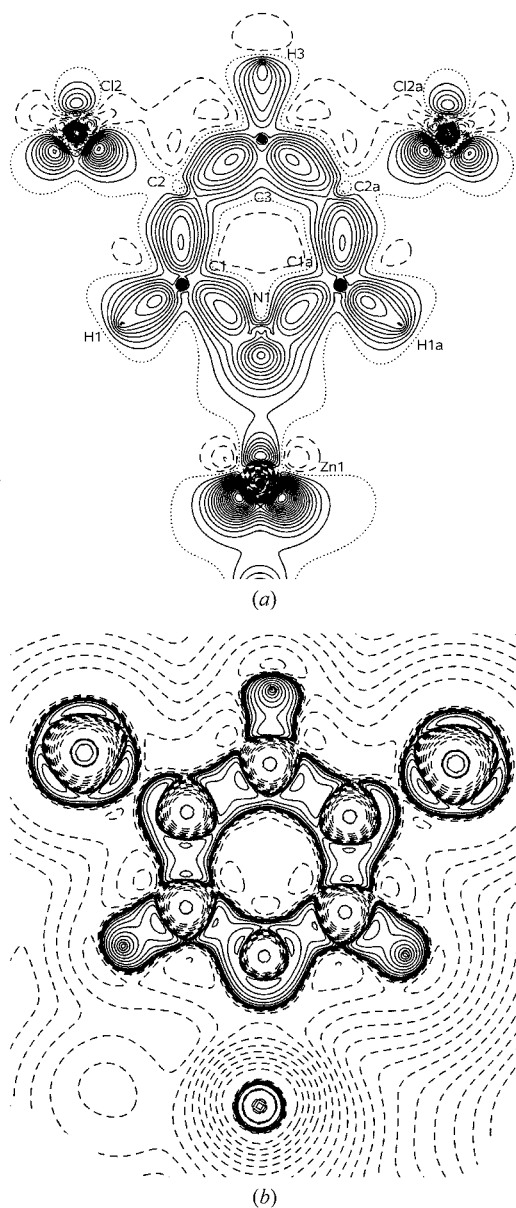


**Figure 2**  
(a) Deformation electron density (intervals at  $0.1 \text{ e } \text{Å}^{-3}$ , excess density solid) and (b) Laplacian of the electron density at  $[\pm 2'' \times 10^{-3} \text{ e } \text{Å}^{-5}$  ( $0 \leq n \leq 20$ , negative values solid)] in the plane of the pyridine ligand in (1).

extend along the direction of the shortest lattice parameter. The apical positions in the pseudo-octahedron around each metal center are occupied by the N atoms of two donor ligands. Single-crystal X-ray diffraction experiments provided intensity data of high resolution which allowed a topological analysis of the electron density following the Atoms In Molecules (AIM) approach (Bader, 1990). We will first address chemical bonding within the polymer strands and later discuss weaker interatomic interactions. The chain polymers (1)–(3) and (5) are isomorphous; they crystallize in the non-centrosymmetric space group  $P4b2$  with similar lattice parameters. The metal centers are located on special positions of  $D_2$  (222) site symmetry. The cation, the pyridine nitrogen and the carbon atom in the *para* position share the same twofold axis, and the metal is situated in the plane of the pyridine for symmetry reasons. The topological analysis confirms (3, -1) critical points for the conventional chemical bonds in all solids under study. As an example, Fig. 2 shows the deformation density (*a*) and the negative Laplacian  $\nabla^2\rho$  of the electron density (*b*) for the Zn-pyridine plane in compound (1). In agreement with the expectation for covalent interactions, C–C and C–N bonds in the heterocyclic ligand are characterized by negative values for  $\nabla^2\rho$  at the bond critical points.

Information concerning the bonding characteristics in the halide-bridged metal backbone in these chain polymers is given in Fig. 3: Both deformation density (*a*) and Laplacian (*b*) are shown for the  $[\text{Zn}(\mu\text{-Cl})_2]_\infty$  section of (1).

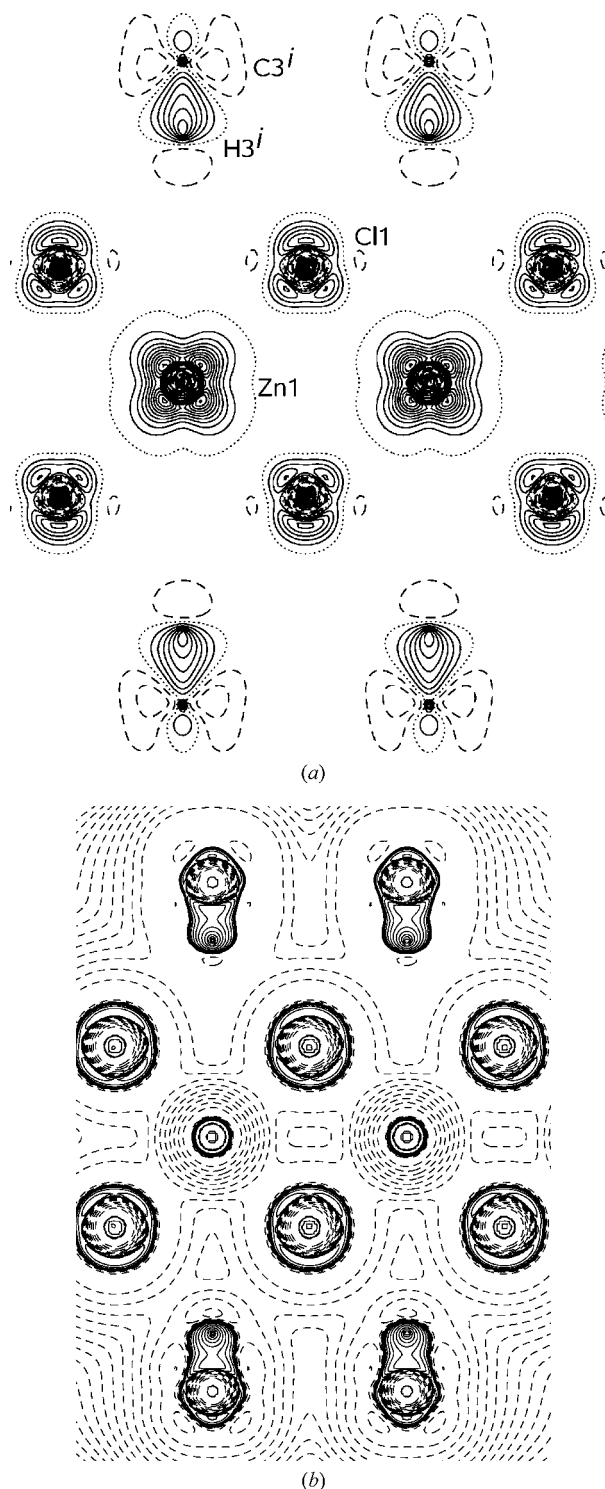
Compound (4) also shows a chain polymer with apparently related structural features; however, the lower space-group symmetry is in agreement with a less regular arrangement and hence suggests a separate discussion. Compound (4) contains two symmetrically independent polymer strands which differ significantly with respect to metal coordination: In one of the chains, coordination of the metal by the pyridine ligands is unexceptional, with N and *para* C atoms of the pyridine ligands (4g site) and the metal on the same crystallographic twofold axis. This situation is depicted in Fig. 4.

In contrast to this situation, N,  $C_{\text{para}}$  (4i site) and the Cd cation in the second strand occupy the same crystallographic mirror plane; this plane is perpendicular to the least-squares plane through the heteroaromatic ring. The metal is situated 0.8277 (15) Å out of the ring plane (Figs. 5*a* and *b*) and hence is hardly visible in a deformation-density plot through this ligand (Fig. 5*c*). A comparison of the Laplacians in the region of the metal–N bonds shows the orientation of the nitrogen lone pair in the pyridine plane in the former (Fig. 4*b*) and out of that plane in the latter (Fig. 5*b*) polymer strand. The angle  $\delta$  subtended by the N1-lone pair vector and the Cd1–N1 bond amounts to *ca* 10°.

We had encountered comparable out-of-plane coordination in the low-temperature phase of  $[\text{Pb}(\mu\text{-Cl})_2(\mu\text{-bipy})]_\infty$  (Hu & Englert, 2006*a,b*) and for a polymer of the higher homologue mercury (Hu *et al.*, 2007).

In Table 3, a compilation of criteria associated with ‘conventional’, *i.e.* covalent and coordination bonds in all compounds under study is provided. The electron density in the bond-critical point doubtless represents an important

quantity which characterizes the significance of an interatomic interaction. A second widely used classification of chemical bonds relies on the Laplacian; usually covalent bonds are associated with negative values for  $\nabla^2\rho$  at the bond-critical

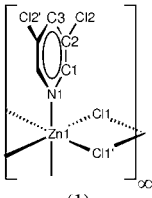
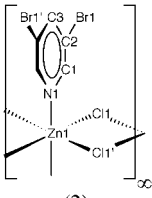
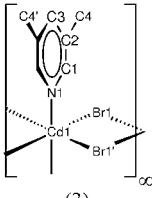
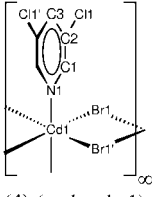
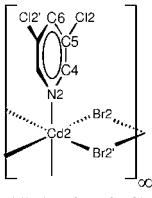
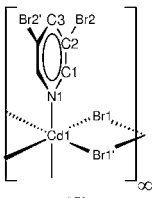


**Figure 3**  
(*a*) Deformation electron density (intervals at  $0.1 \text{ e } \text{\AA}^{-3}$ , excess density solid) and (*b*) Laplacian of the electron density [ $\pm 2^n \times 10^{-3} \text{ e } \text{\AA}^{-5}$  ( $0 \leq n \leq 20$ ), negative values solid] in [001] direction at height  $z = 0.5$ , in the plane of the metal cations and bridging halides in (1). In both representations, neighbouring polymer chains interacting via *para*-C–H... $\mu$ -Cl interactions are included. Symmetry operator (i)  $y, 1-x, -z$ .

**Table 3**

Atom-labelling scheme and properties of bond-critical points in conventional bonds in (1)–(5).

$d_1$  and  $d_2$  are distances from the first and second atom to the (3, -1) critical point,  $R_{ij}$  denotes the sum  $d_1 + d_2$  and may be compared to the interatomic distance,  $\rho_{CP}$  is the electron density,  $\nabla^2\rho_{CP}$  is the Laplacian of the electron density.  $G$  and  $V$  are kinetic energy density and potential energy density (in atomic units, hartree bohr<sup>-3</sup>),  $G(r_c)/\rho$  is the ratio between kinetic energy density and electron density (in atomic units, hartree e<sup>-1</sup>).

Compound	Bond	Interatomic distance (Å)	$R_{ij}$ (Å)	$d_1$ (Å)	$d_2$ (Å)	$\rho_{CP}$ (e Å <sup>-3</sup> )	$\nabla^2\rho_{CP}$ (e Å <sup>-5</sup> )	$G(r_c)$ (a.u.)	$V(r_c)$ (a.u.)	$G(r_c)/\rho$ (a.u.)
 (1)	Zn1—Cl1	2.48573 (11)	2.508	1.183	1.325	0.257 (2)	3.878 (4)	0.039	-0.038	1.029
	Zn1—N1	2.1923 (7)	2.192	1.043	1.150	0.350 (6)	6.610 (6)	0.066	-0.064	1.280
	Cl2—C2	1.7282 (6)	1.730	1.002	0.728	1.28 (4)	0.17 (12)	0.180	-0.359	0.953
	N1—C1	1.3447 (7)	1.346	0.802	0.544	2.48 (5)	-30.8 (3)	0.328	-0.976	0.892
	C1—C2	1.3950 (8)	1.395	0.702	0.693	2.29 (5)	-22.5 (2)	0.317	-0.867	0.937
	C2—C3	1.3944 (7)	1.397	0.740	0.656	2.25 (5)	-24.1 (2)	0.306	-0.862	0.879
	C1—H1	1.083	1.083	0.764	0.319	1.95 (9)	-20.1 (4)	0.223	-0.655	0.772
	C3—H3	1.083	1.083	0.703	0.380	1.75 (5)	-18.4 (2)	0.175	-0.541	0.675
 (2)	Zn1—Cl1	2.4984 (3)	2.500	1.127	1.372	0.238 (3)	4.261 (2)	0.040	-0.037	1.144
	Zn1—N1	2.1929 (18)	2.193	1.056	1.137	0.349 (13)	5.999 (15)	0.062	-0.062	1.200
	Br1—C2	1.8866 (19)	1.892	1.069	0.824	1.25 (7)	-5.90 (18)	0.132	-0.325	0.712
	N1—C1	1.343 (2)	1.349	0.722	0.627	2.44 (12)	-30.5 (5)	0.315	-0.946	0.872
	C1—C2	1.386 (2)	1.392	0.731	0.662	2.18 (11)	-12.2 (4)	0.352	-0.831	1.089
	C2—C3	1.390 (2)	1.414	0.748	0.666	2.15 (9)	-17.9 (2)	0.302	-0.790	0.949
	C1—H1	1.083	1.088	0.761	0.328	1.79 (12)	-19.1 (5)	0.182	-0.562	0.686
	C3—H3	1.083	1.083	0.846	0.237	1.98 (8)	-41.7 (5)	0.083	-0.599	0.283
 (3)	Cd1—Br1	2.7676 (2)	2.773	1.321	1.452	0.208 (3)	2.768 (3)	0.028	-0.027	0.903
	Cd1—N1	2.3565 (14)	2.357	1.218	1.138	0.325 (11)	6.223 (12)	0.061	-0.058	1.273
	C4—C2	1.504 (3)	1.506	0.862	0.644	1.69 (12)	-13.1 (5)	0.194	-0.524	0.778
	N1—C1	1.339 (2)	1.341	0.754	0.588	2.50 (15)	-20.4 (7)	0.407	-1.026	1.098
	C1—C2	1.391 (2)	1.396	0.746	0.650	2.15 (13)	-16.5 (5)	0.312	-0.795	0.980
	C2—C3	1.388 (2)	1.393	0.829	0.564	2.12 (10)	-23.6 (5)	0.229	-0.703	0.806
	C1—H1	1.083	1.090	0.780	0.310	1.63 (12)	-14.3 (5)	0.170	-0.488	0.703
	C3—H3	1.083	1.083	0.718	0.366	1.58 (7)	-14.5 (3)	0.155	-0.460	0.661
 (4) (molecule 1)	Cd1—Br1	2.7325 (2)	2.733	1.316	1.417	0.211 (3)	3.223 (2)	0.031	-0.029	0.997
	Cd1—N1	2.390 (3)	2.390	1.218	1.172	0.333 (4)	5.927 (5)	0.060	-0.059	1.216
	Cl1—C2	1.7225 (18)	1.723	0.962	0.760	1.45 (5)	-3.44 (10)	0.197	-0.430	0.918
	N1—C1	1.333 (2)	1.336	0.812	0.524	2.49 (12)	-29.7 (5)	0.339	-0.985	0.919
	C1—C2	1.391 (2)	1.393	0.796	0.597	2.19 (7)	-18.2 (3)	0.313	-0.815	0.966
	C2—C3	1.391 (2)	1.391	0.758	0.633	2.22 (6)	-18.2 (2)	0.324	-0.836	0.984
	C1—H1	1.083	1.085	0.749	0.335	1.77 (8)	-14.9 (3)	0.205	-0.565	0.782
	C3—H3	1.083	1.083	0.786	0.298	1.74 (6)	-15.3 (3)	0.194	-0.547	0.751
 (4) (molecule 2)	Cd2—Br2	2.7305 (2)	2.741	1.345	1.396	0.180 (4)	2.921 (3)	0.027	-0.024	1.013
	Cd2—N2	2.384 (2)	2.384	1.227	1.158	0.329 (5)	6.096 (5)	0.061	-0.059	1.247
	Cl2—C5	1.7272 (17)	1.727	0.967	0.760	1.33 (5)	0.18 (10)	0.192	-0.383	0.978
	N2—C4	1.339 (2)	1.344	0.851	0.493	2.32 (13)	-20.9 (5)	0.339	-0.896	0.987
	C4—C5	1.393 (2)	1.395	0.711	0.683	2.17 (6)	-16.3 (2)	0.320	-0.809	0.995
	C5—C6	1.384 (2)	1.384	0.604	0.781	2.14 (10)	-16.4 (3)	0.310	-0.790	0.976
	C4—H4	1.083	1.084	0.732	0.352	1.92 (7)	-17.9 (3)	0.229	-0.644	0.805
	C6—H6	1.083	1.083	0.808	0.275	1.96 (6)	-26.5 (4)	0.182	-0.638	0.627
 (5)	Cd1—Br1	2.7360 (2)	2.747	1.309	1.438	0.188 (4)	2.953 (3)	0.028	-0.025	0.997
	Cd1—N1	2.3872 (11)	2.387	1.238	1.149	0.253 (12)	5.432 (13)	0.050	-0.043	1.323
	Br2—C2	1.8821 (13)	1.891	1.073	0.817	1.13 (7)	-3.1 (2)	0.124	-0.281	0.743
	N1—C1	1.3380 (18)	1.346	0.793	0.553	2.4 (2)	-32.9 (7)	0.284	-0.910	0.800
	C1—C2	1.3875 (19)	1.388	0.664	0.725	2.3 (2)	-21.3 (5)	0.330	-0.880	0.967
	C2—C3	1.3918 (18)	1.398	0.769	0.629	2.11 (8)	-12.4 (2)	0.327	-0.783	1.047
	C1—H1	1.083	1.084	0.756	0.328	1.98 (14)	-20.2 (5)	0.232	-0.673	0.790
	C3—H3	1.083	1.083	0.643	0.440	1.74 (8)	-17.5 (3)	0.179	-0.539	0.692

points, whereas closed-shell interactions such as ionic bonds or van der Waals contacts show positive  $\nabla^2\rho$ . In particular, for bonds between very different atom types, however, the sign of the Laplacian alone does not necessarily represent a reliable criterion (Macchi *et al.*, 1998). In view of these limitations, estimates for the kinetic energy densities in the (3, -1) critical points have been derived following the procedure of Abramov (1997) and have also been included in Table 3, together with

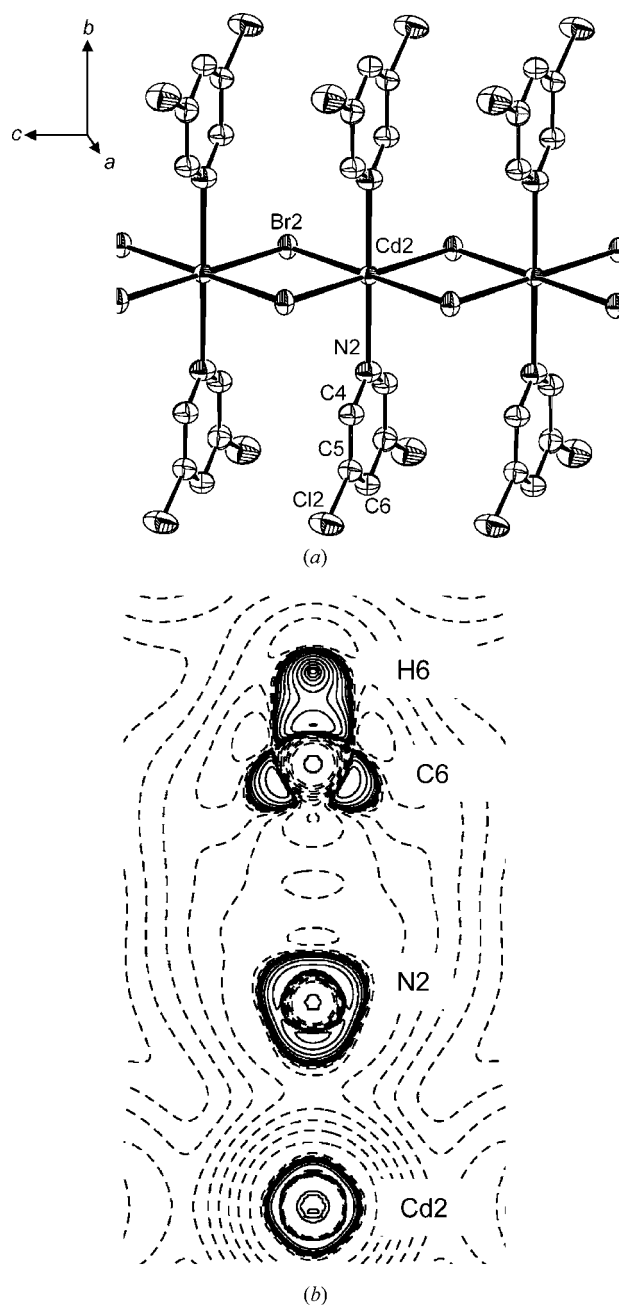


**Figure 4**  
In-plane metal coordination by pyridine in one of the two symmetrically independent polymer strands in (4). The site symmetry of the Cd center is  $2/m$ . (a) Displacement ellipsoid plot (90% probability, H atoms omitted); (b) Laplacian of the electron density [ $\pm 2^n \times 10^{-3} \text{ e \AA}^{-5}$  ( $0 \leq n \leq 20$ ), negative values solid] in the region of the Cd2–N2 bond; the view direction is in the plane through the pyridine ring and perpendicular to Cd2–N2.

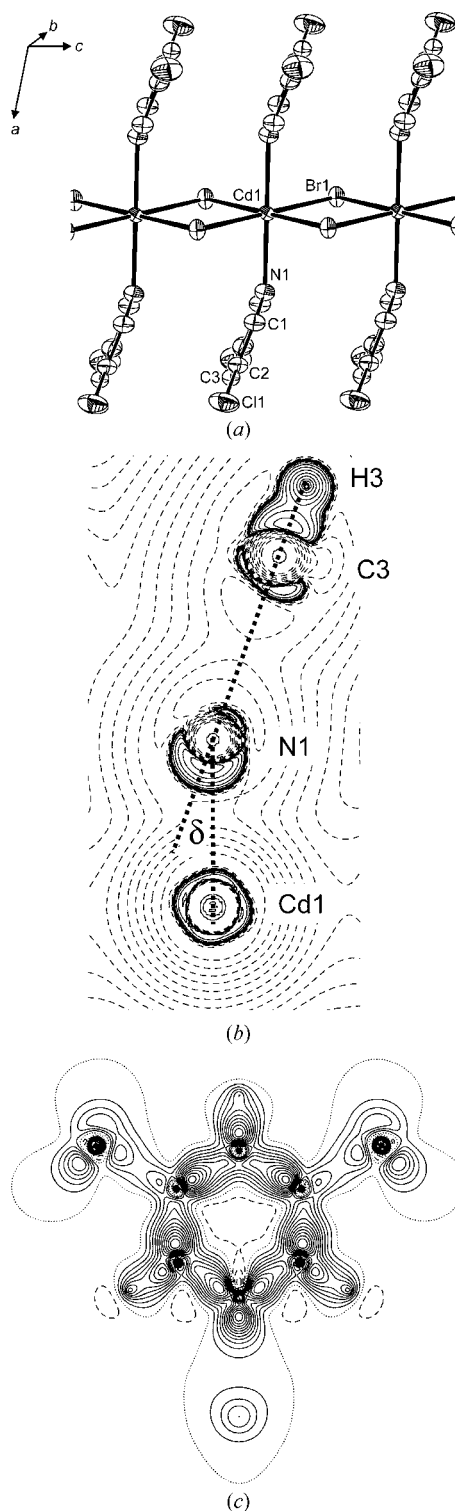


**Figure 5**  
Out-of-plane metal coordination by pyridine in one of the two symmetrically independent polymer strands in (4). The site symmetry of the Cd center is  $2/m$ . (a) Displacement ellipsoid plot (90% probability, H atoms omitted); (b) Laplacian of the electron density [ $\pm 2^n \times 10^{-3} \text{ e \AA}^{-5}$  ( $0 \leq n \leq 20$ ), negative values solid] in the region of the Cd1–N1 bond; the view direction is in the plane through the pyridine ring and perpendicular to Cd1–N1; (c) Deformation density in the plane of the pyridine ligand (intervals at  $0.1 \text{ e \AA}^{-3}$ , excess density solid).

the potential energy according to the local virial theorem (Espinosa *et al.*, 1998) and the ratio between kinetic energy and electron density in the bond-critical point. Trends in these criteria for classifying chemical bonds in (1)–(5) will be discussed below.

All metal–nitrogen coordinative bonds can consistently be characterized by electron densities around  $0.3 \text{ e } \text{Å}^{-3}$  in the bond-critical points and values of  $\sim 6 \text{ e } \text{Å}^{-5}$  for the Laplacian. They are also rather similar with respect to energy densities ( $|V| \simeq G$ ) and, necessarily, the derived quantity  $G/\rho$ .

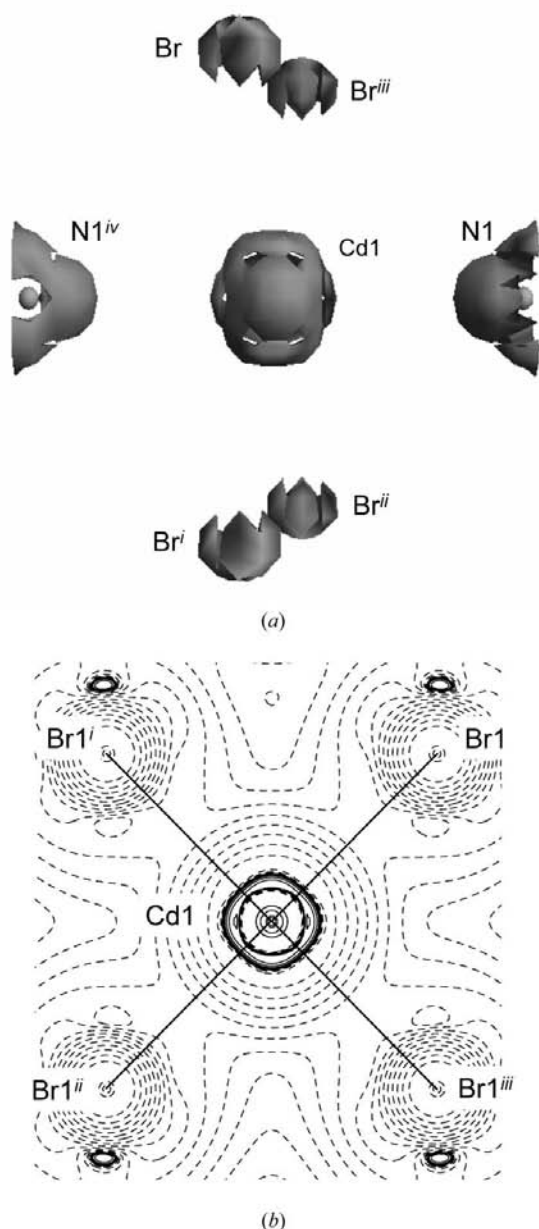


**Figure 6**

(a) Isosurface showing the negative Laplacian of the experimental charge density at  $-\nabla^2\rho = 10 \text{ e } \text{Å}^{-5}$  in (4) (molecule 1). (b) Laplacian of the electron density [ $\pm 2^n \times 10^{-3} \text{ e } \text{Å}^{-5}$  ( $0 \leq n \leq 20$ ), negative values solid] in the equatorial plane of the distorted coordination octahedron around Cd1. Symmetry operators for both views (i)  $x, y, z - 1$ ; (ii)  $-x, -y, -z$ ; (iii)  $-x, -y, 1 - z$ ; (iv)  $-x, y, -z$ ;

According to these criteria the  $M-N$  interactions may be classified as essentially ionic; neither the different cations involved [Zn–N in (1) and (2), Cd–N in (3)–(5)], nor the different substituents at the ligands induce a qualitative change in the bonding characteristics. The more pronounced polarization of the larger and softer  $\text{Cd}^{2+}$  cations will be discussed below. Information about experimental electron density in comparable coordination compounds is limited and confirms that the commonly reported values of experimental electron density and Laplacian in the bond-critical point are not very sensitive criteria for bonds between transition metals and donor ligands. The electronic features of the Zn–N bond in the cationic complex bis(thiosemicarbazide)zinc(II) have recently been reported (Novakovic *et al.*, 2007): The zinc–nitrogen bond in this tetrahedral complex from the literature is shorter than in our polymers (1) and (2) in which the metal is in distorted octahedral coordination, and it shows a higher electron density of  $0.5 \text{ e } \text{Å}^{-3}$  in the bond-critical points, but a similar value of  $7 \text{ e } \text{Å}^{-5}$  for the Laplacian. A larger number of interactions between a Zn center and coordinated atoms from the second period occur in the organometallic compound bis[1,2( $\eta^5$ )-pentamethylcyclopentadienyl]dizinc which, however, features Zn–C rather than Zn–N bonds. A recent charge-density study finds  $\rho = 0.4 \text{ e } \text{Å}^{-3}$  and  $\nabla^2\rho = 2 \text{ e } \text{Å}^{-5}$  for the average value of the Zn–C (3, –1) critical points in this compound (Van der Maelen *et al.*, 2007). Comparisons with literature data are even more difficult to make for the Cd–N bonds in (3)–(5): we are not aware of any charge-density study on a cadmium derivative. For the second-series transition-metal derivative ethylenebis(1-indenyl)zirconium dichloride Stash *et al.* (2005) reported  $\rho = 0.3 \text{ e } \text{Å}^{-3}$  and  $\nabla^2\rho = 4 \text{ e } \text{Å}^{-5}$  for the Zr–C bond. Hashizume and coworkers have found very similar features for the Zr–C bond topology in a zirconium organic compound without any halide ligand (Hashizume *et al.*, 2006). An investigation on silver acetylene complexes revealed an electron density of  $0.5 \text{ e } \text{Å}^{-3}$  at the (3, –1) critical point between the metal cation and the C–C triple bond (Reisinger *et al.*, 2007).

The Zn–Cl interactions in (1) and (2) differ significantly from the Cd–Br bonds in (3)–(5): the former are characterized by a higher positive value for the Laplacian and a slightly lower electron density than the latter. In the Zn–Cl case, the bond-critical point is significantly closer to Zn than to Cl, whereas it is located approximately half-way along the metal–halide bond path for the Cd–Br bonds.

With respect to carbon–halide bonds, the Laplacian varies between +0.18 (10) [C–Cl in (4)] and  $-5.90$  (18) [C–Br in (2)] and does not represent a straightforward criterion for classification; in contrast the comparison between kinetic energy density  $G$  and potential energy  $V$  consistently results in  $|V| > G$  and underlines that these bonds represent shared interactions. This assignment is corroborated by the fact that the ratio  $G(r_c)/\rho$  is less than unity for all carbon–halide bonds (Abramov, 1997).

Chemical intuition suggests that the C–N and C–C bonds are covalent; they are all associated with negative values for the Laplacian of the electron density, and the potential energy



**Table 4**

Properties of (3, -1) critical points in secondary interactions in (1)–(5).

$d_1$  and  $d_2$  are distances from the first and second atom to the critical point,  $R_{ij}$  denotes the sum  $d_1 + d_2$  and may be compared with the interatomic distance,  $\rho_{CP}$  is the electron density,  $\nabla^2\rho_{CP}$  is the Laplacian of the electron density.

Compound	Interaction and type	Interatomic distance (Å)	$R_{ij}$ (Å)	$d_1$ (Å)	$d_2$ (Å)	$\rho_{CP}$ (e Å <sup>-3</sup> )	$\nabla^2\rho_{CP}$ (e Å <sup>-5</sup> )
(1)	H1···Cl1 <i>intra</i>	2.55	2.57	0.97	1.60	0.102 (7)	1.219 (2)
	C2···Cl2 <sup>i</sup> <i>intra</i>	3.5217 (7)	3.523	1.786	1.737	0.047 (3)	0.443 (2)
	Cl2···Cl2 <sup>i</sup> <i>inter</i>	3.7641 (3)	3.764	1.888	1.877	0.023 (2)	0.307 (2)
	H3···Cl1 <sup>vi</sup> <i>inter</i>	2.69	2.73	1.01	1.72	0.056 (5)	0.768 (3)
(2)	Br1···Br1 <i>intra</i>	3.7044 (2)	3.705	1.837	1.869	0.042 (2)	0.603 (2)
	H1···Cl1 <i>intra</i>	2.59	2.67	1.08	1.59	0.092 (6)	0.980 (3)
	C2···Br1 <sup>i</sup> <i>intra</i>	3.5482 (19)	3.571	1.811	1.760	0.045 (3)	0.469 (3)
	C2···C2 <sup>i</sup> <i>intra</i>	3.704 (3)	3.711	1.958	1.752	0.047 (5)	0.377 (2)
	Br1···Br1 <sup>ii</sup> <i>inter</i>	3.5834 (2)	3.608	1.898	1.710	0.038 (3)	0.456 (5)
	H3···Cl1 <sup>iv</sup> <i>inter</i>	2.75	2.86	1.06	1.80	0.034 (5)	0.461 (2)
(3)	H1···Br1 <i>intra</i>	2.77	2.83	1.04	1.79	0.086 (7)	0.851 (4)
	H3···Br1 <sup>iv</sup> <i>inter</i>	2.85	2.91	1.03	1.88	0.051 (5)	0.577 (2)
(4)	Cl1···Cl1 <sup>i</sup> <i>intra</i>	3.8561 (6)	3.858	1.937	1.921	0.023 (2)	0.310 (2)
	Cl2···Cl2 <sup>i</sup> <i>intra</i>	3.8561 (6)	3.861	1.912	1.949	0.023 (2)	0.290 (2)
	H1···Br1 <i>intra</i>	3.26	3.32	1.32	2.00	0.029 (2)	0.320 (2)
	H4···Br2 <sup>viii</sup> <i>intra</i>	2.81	2.86	1.09	1.77	0.063 (4)	0.733 (2)
	Cl2···Cl1 <sup>i</sup> <i>inter</i>	3.7622 (6)	3.764	1.875	1.889	0.025 (2)	0.325 (2)
	Cl2···Cl1 <sup>v</sup> <i>inter</i>	3.6525 (6)	3.653	1.826	1.827	0.032 (2)	0.418 (2)
	H6···Br1 <i>inter</i>	2.78	2.83	1.05	1.78	0.055 (5)	0.627 (2)
	H3···Br2 <sup>vii</sup> <i>inter</i>	2.69	2.70	1.00	1.70	0.067 (9)	0.701 (3)
(5)	Br2···Br2 <sup>i</sup> <i>intra</i>	3.9082 (2)	3.908	1.946	1.963	0.040 (2)	0.547 (2)
	C2···C2 <sup>i</sup> <i>intra</i>	3.9082 (2)	3.945	1.984	1.961	0.032 (3)	0.276 (2)
	H1···Br1 <i>intra</i>	2.80	2.83	1.11	1.72	0.071 (7)	0.701 (4)
	Br2···Br2 <sup>iii</sup> <i>inter</i>	3.8973 (3)	3.903	2.015	1.888	0.028 (2)	0.267 (3)

Symmetry codes: (i)  $x, y, 1 + z$ ; (ii)  $1 - y, x, -z$ ; (iii)  $y, 1 - x, 2 - z$ ; (iv)  $1 - y, x, 2 - z$ ; (v)  $\frac{1}{2} - x, \frac{1}{2} - y, -z$ ; (vi)  $y, 1 - x, -z$ ; (vii)  $\frac{1}{2} + x, -\frac{1}{2} + y, -1 + z$ ; (viii)  $-x, y, 1 - z$ .

density in the bond-critical point systematically overcompensates the kinetic energy density.

Figs. 4(b) and 5(b) indicate a non-spherical charge distribution for the Cd centers in (4). The Laplacians for both symmetrically independent molecules show local charge concentrations in the direction of the Cd–N bonds. A closer inspection of this feature is possible based on Fig. 6(a), which shows the isosurface of the negative Laplacian of the experimental charge density around cation Cd1 in (4). A different

intrastrand *ortho*-C–H··· $\mu$ -X contacts in all compounds and interstrand *para*-C–H··· $\mu$ -X interactions in the halopyridine derivatives (1), (2), (4) and (5). In order to document an example for the latter both with respect to deformation density and Laplacian, the *para*-C–H··· $\mu$ -Cl contacts in (1) have been included in Fig. 3. Shortest contacts correspond to hydrogen···acceptor distances of *ca* 2.6 Å for C–H···Cl and *ca* 2.8 Å for C–H···Br.

Halogen bonding can also be expected to play a role in stabilizing the structures with halogen-substituted ligands: In (1), (2), (4) and (5) interhalogen contacts involving substituents on neighbouring pyridine ligands occur. The corresponding distances amount to the shortest lattice parameters and fall in the range of van der Waals contacts; we note that the very popular compilation of Bondi (1.75 Å for Cl, 1.85 Å for Br; Bondi, 1964) and that published more recently by Batsanov (1.8 Å for Cl, 1.9 Å for Br; Batsanov, 1995) essen-

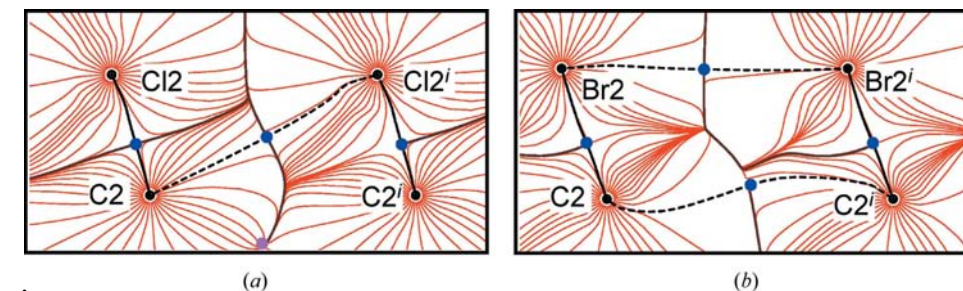


**Figure 7**

Bond paths between neighbouring pyridine rings along the polymer chain in (a) (1) and (b) (5). Gradient trajectories (red) and (3, -1) critical points (blue) in the plane defined by  $C_{meta}$  of the pyridine ring, its halogen substituent, and the corresponding symmetry-equivalent atoms defined by the symmetry operator (i)  $x, y, 1 + z$ . This figure is in colour in the electronic version of this paper.

tially agree with respect to the elements under discussion.

Both secondary interactions discussed above, non-classical hydrogen bonds and halogen bonding, are reflected in local features of the electron density; Table 4 provides a summary of distances, symmetry operations and electron densities in the (3, -1) critical points identified.

Table 4 shows that the electron density at the (3, -1) critical point for the non-classical hydrogen bonds ranges between 0.10 and 0.03 e Å<sup>-3</sup>. Two recent reports covering C—H···O interactions report  $\rho = 0.03$  e Å<sup>-3</sup> (Munshi *et al.*, 2006) and  $\rho = 0.02$ –0.07 e Å<sup>-3</sup> (Hübschle *et al.*, 2008) and find small positive values for the Laplacian, also consistent with our results. For our C—H···X contacts, the highest electron densities are encountered for intra-strand non-classical hydrogen bonds between the H atom attached to C<sub>ortho</sub> in the substituted

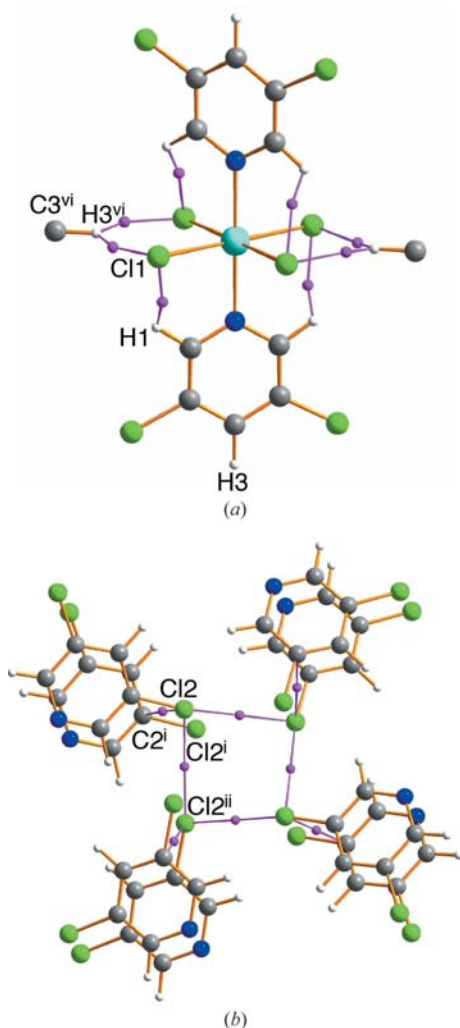


**Figure 8**

Secondary interactions in (1). View directions are slightly tilted with respect to [001], (3, -1) critical points are represented as small magenta-coloured spheres. (a) Intrastrand C<sub>ortho</sub>—H1···Cl1 and interstrand C<sub>para</sub>—H3<sup>vi</sup>···Cl1 interactions. (b) Interstrand Cl2···Cl2<sup>i</sup>/Cl2···C2<sup>i</sup> contacts [for these interactions, (3, -1) critical points merge] and Cl2···Cl2<sup>ii</sup> contacts in the four-membered homodromic cycle. Only the pyridine substituents are shown, Zn and bridging chloride atoms have been omitted. This figure is in colour in the electronic version of this paper.

pyridines and the bridging halides. In agreement with the situation for classical hydrogen bonds (Mínguez Espallargas *et al.*, 2008), M—Cl···H—C are associated with higher values for  $\rho$  than M—Br···H—C.

The compounds with 3,5 dihalogen substitution at the pyridine ligands differ with respect to the secondary interactions along the chain direction: Fig. 7 shows that no (3, ±1) critical point is detected along the polymer strand between chlorine substituents on adjacent pyridine ligands in (1), whereas a direct bond path between the halide atoms shows up in the gradient trajectory in the Cd<sup>II</sup> chain polymer (5). In other words: at least the unusual Zn<sup>II</sup> polymer (1) does not owe its existence to stabilizing halogen bonds in chain direction; however, a favourable interaction along the strands is due to C2···Cl2<sup>i</sup>. Gradient trajectory plots for the other coordination polymers with potential intrastrand halogen interactions (2) and (4) (two symmetrically independent chains) are provided in the supporting information.

According to the ideas of Desiraju and coworkers (Pedirreddi *et al.*, 1994), halogen bonding between orthogonal C—X donors and acceptors should be particularly effective for polarizable X, *i.e.* more important for secondary interactions between bromo than chloro substituents. This situation is reflected in interstrand contacts between halogen substituents on pyridine in neighbouring chains which amount to the shortest Br···Br distances of 3.5836 (2) Å in (2) and slightly longer Cl···Cl distances such as 3.6535 (5) Å in (4). In agreement with the concept of halogen bonding, the overall space filling is the lowest for the only compound necessarily lacking this interaction, namely the dimethylpyridine derivative (3) (*cf.* Table 2). We also note that (3) shows the lowest thermal stability. These observations should, however, not be overestimated in their significance in view of the fact that only five derivatives have been studied in this context.

Fig. 8 provides a graphical summary of the (3, -1) critical points associated with secondary interactions in (1).

## 5. Conclusion

The determination of experimental electron densities for the five coordination polymers studied in this work had to face the problems of low suitability factors for (2)–(5) and non-centrosymmetric space groups for (1), (2), (3) and (5). However, results at the IAM level were excellent and the agreement between the multipole refinement results from datasets obtained for different but chemically related compounds was encouraging. We have shown that the topologies of the experimental electron densities, based on high-resolution diffraction experiments for (1)–(5), are consistent and that they are in agreement with intuitive chemical concepts of weak interactions such as hydrogen bonds and interhalogen contacts. Secondary interactions initially suggested based on distance criteria could be associated with (3, -1) critical points. Contrary to our earlier entirely geometric interpretation, intrastrand C—H···X contacts are associated with the largest electron densities in the critical points: their value of *ca* 0.1 e Å<sup>-3</sup> comes close to the electron

density determined for classical moderately strong N—H···N bonds (Munshi *et al.*, 2006). At the same time, our results indicate that the contribution of the closed-shell interactions between halogen substituents on adjacent pyridine ligands along the same chain only plays a minor role. Future work will address interactions in mononuclear zinc complexes of elemental composition comparable to (1) and (2).

The analysis of a wide variety of weaker interactions and their use in designing extended structures is an area of active research, and it is of interest to know how meaningful charge-density studies can be in that context. The significance of experimental results for weak interactions has been challenged under two different aspects: for hydrogen bonds Spackman (1999) has shown that information about energy densities based on multipole refinements does not differ significantly from results obtainable from much simpler spherical electron densities. The experimentalist may ask whether a full charge-density study is appropriate if its focus is on weak interactions rather than on more conventional chemical bonds. The worst-case scenario would be that the charge density study does not provide any information beyond a standard diffraction experiment. Gatti and coworkers (Gatti *et al.*, 2002) have addressed the question in which cases the crystallographic standard model and more elaborate charge-density determinations give such an agreement. According to their results, the topological analysis can be used to distinguish between bonding and non-bonding contacts; in the case of the former, topologies and energy densities based on spherical and multipole models agree well. If we adopt this view of Spackman and Gatti in reconsidering our results, the topology of the experimental electron density can help to distinguish between more and less important interactions. With respect to (1), one may find that non-classical hydrogen bonds are more important than interhalogen contacts along the chain; the topological properties of the interactions classified as bonding will probably not differ much from those obtained with a spherical model. The criticism raised by Dunitz & Gavezzotti (2005) is more fundamental: they have emphasized the fact that intermolecular interactions occur between charge distributions rather than between individual atoms. Contacts between certain individual atoms, for example connected by strong hydrogen bonds, may well be decisive; in many cases of weak interactions, however, care must be taken not to overestimate the relevance of short contacts based on their mere existence. The worst-case scenario according to Dunitz and Gavezzotti could imply that both a charge-density study and a conventional diffraction experiment at moderate resolution just ask the wrong question when they try to spot specific weak interactions.

The authors thank Dr Birger Dittrich and Dipl. Chem. Julian Holstein for many hours of helpful discussion and Mrs Irmgard Kalf for her continuing assistance with the crystallization of the compounds. Professor E. Espinosa has been most helpful with his suggestion to analyze interstrand halogen bonding in terms of a topological analyses. This work

was supported by DFG, priority program 1178, Experimental Charge Density as the Key to Understand Chemical Interactions.

## References

- Abramov, Yu. A. (1997). *Acta Cryst.* **A53**, 264–272.
- Bader, R. F. W. (1990). *Atoms in Molecules: A Quantum Theory*. Oxford University Press.
- Batsanov, S. S. (1995). *Izv. Akad. Nauk Ser. Khim.* pp. 24–29.
- Bhosekar, G., Jeß, I., Lehnert, N. & Näther, C. (2008). *Eur. J. Inorg. Chem.* pp. 605–611.
- Blessing, R. H. (1995). *Acta Cryst.* **A51**, 33–38.
- Bondi, A. (1964). *J. Phys. Chem.* **68**, 441–451.
- Bruker (2003). *SAINT*, Version 6.45. Bruker AXS Inc., Madison, Wisconsin, USA.
- Coppens, P. (1977). *Isr. J. Chem.* **16**, 144–148.
- Dunitz, J. D. & Gavezzotti, A. (2005). *Angew. Chem. Int. Ed.* **44**, 1766–1787.
- Englert, U. & Schiffrs, S. (2006a). *Acta Cryst.* **E62**, m194–m195.
- Englert, U. & Schiffrs, S. (2006b). *Acta Cryst.* **E62**, m295–m296.
- Espinosa, E., Molins, E. & Lecomte, C. (1998). *Chem. Phys. Lett.* **285**, 170–173.
- Farrugia, L. J., Frampton, C. S., Howard, J. A. K., Mallinson, P. R., Peacock, R. D., Smith, G. T. & Stewart, B. (2006). *Acta Cryst.* **B62**, 236–244.
- Flack, H. D. (1983). *Acta Cryst.* **A39**, 876–881.
- Gatti, C., May, E., Destro, R. & Cargnoni, F. (2002). *J. Phys. Chem. A*, **106**, 2707–2720.
- Gavezzotti, A. (1983). *J. Am. Chem. Soc.* **105**, 5220–5225.
- Hansen, N. K. & Coppens, P. (1978). *Acta Cryst.* **A34**, 909–921.
- Hashizume, D., Suzuki, N. & Chihara, T. (2006). *Chem. Commun.* pp. 1233–1235.
- Hu, C. & Englert, U. (2001a). *CrystEngComm*, **3**, 91–95.
- Hu, C. & Englert, U. (2001b). *Acta Cryst.* **C57**, 1251–1252.
- Hu, C. & Englert, U. (2002). *CrystEngComm*, **4**, 20–25.
- Hu, C. & Englert, U. (2005a). *Angew. Chem.* **117**, 2321–2323.
- Hu, C. & Englert, U. (2005b). *Angew. Chem. Int. Ed.* **44**, 2281–2283.
- Hu, C. & Englert, U. (2006a). *Angew. Chem.* **118**, 3535–3538.
- Hu, C. & Englert, U. (2006b). *Angew. Chem. Int. Ed.* **45**, 3457–3459.
- Hu, C., Huster, J. & Englert, U. (2003). *Z. Kristallogr.* **218**, 761–765.
- Hu, C., Kalf, I. & Englert, U. (2007). *CrystEngComm*, **9**, 603–610.
- Hu, C., Li, Q. & Englert, U. (2003). *CrystEngComm*, **5**, 519–529.
- Hübschle, C. B., Dittrich, B., Grabowsky, S., Messerschmidt, M. & Luger, P. (2008). *Acta Cryst.* **B64**, 363–374.
- Kitaigorodsky, A. I. (1973). *Molecular Crystals and Molecules*. New York, London: Academic Press.
- Macchi, P. & Coppens, P. (2001). *Acta Cryst.* **A57**, 656–662.
- Macchi, P., Proserpio, D. M. & Sironi, A. (1998). *J. Am. Chem. Soc.* **120**, 13429–13435.
- Macchi, P. & Sironi, A. (2003). *Coord. Chem. Rev.* **238–239**, 383–412.
- Meulenaer, J. de & Tompa, H. (1965). *Acta Cryst.* **19**, 1014–1018.
- Mínguez Espallargas, G., Brammer, L., Allan, D. R., Pulham, C. R., Robertson, N. & Warren, J. E. (2008). *J. Am. Chem. Soc.* **130**, 9058–9071.
- Munshi, P., Thakur, T. S., Guru Row, T. N. & Desiraju, G. R. (2006). *Acta Cryst.* **B62**, 118–127.
- Novakovic, S. B., Bogdanovic, G. A., Fraisse, B., Ghermani, N. E., Bouhmaid, N. & Spasojevic de Biré, A. (2007). *J. Phys. Chem. A*, **111**, 13492–13505.
- Pedireddi, V. R., Reddy, D. S., Goud, B. S., Craig, D. C., Rae, A. D. & Desiraju, G. R. (1994). *J. Chem. Soc. Perkin Trans. 2*, pp. 2353–2360.
- Pickardt, J. & Staub, B. (1996). *Z. Naturforsch. B*, **51**, 947–951.

- Reisinger, A., Trapp, N., Krossing, I., Altmannshofer, S., Herz, V., Presnitz, M. & Scherer, W. (2007). *Angew. Chem. Int. Ed.* **46**, 8295–8298.
- Sheldrick, G. M. (2008). *Acta Cryst.* **A64**, 112–122.
- Spackman, M. A. (1999). *Chem. Phys. Lett.* **301**, 425–429.
- Spek, A. L. (2003). *J. Appl. Cryst.* **36**, 7–13.
- Stash, A. I., Tanaka, K., Shiozawa, K., Makino, H. & Tsirelson, V. G. (2005). *Acta Cryst.* **B61**, 418–428.
- Su, Z. & Coppens, P. (1998). *Acta Cryst.* **A54**, 646–652.
- Van der Maelen, J. F., Gutiérrez-Puebla, E., Monge, Á., García-Granda, S., Resa, I., Carmona, E., Fernández-Díaz, M. T., McIntyre, G. J., Pattison, P. & Weber, H.-P. (2007). *Acta Cryst.* **B63**, 862–868.
- Volkov, A., Macchi, P., Farrugia, L. J., Gatti, C., Mallison, P. R., Richter, T. & Koritsanszky, T. (2006). *XD2006*. University of New York at Buffalo, USA.